

# Assessing Ground-Motion Amplitudes and Attenuation for Small-to-Moderate Induced and Tectonic Earthquakes in the Central and Eastern United States

by Abhineet Gupta, Jack W. Baker, and William L. Ellsworth

## ABSTRACT

In this article, we evaluate the ground-motion prediction equations (GMPEs) described by [Atkinson \(2015\)](#) and [Shahjoui and Pezeshk \(2016\)](#) with ground-motion data collected from the central and eastern United States (CEUS). The former GMPE was developed for small-to-moderate events at short hypocentral distances with application to induced earthquakes in eastern North America, using the ground-motion database developed by the Next Generation Attenuation-West2 (NGA-West2) project ([Bozorgnia et al., 2014](#)). The latter GMPE was developed for the central and eastern North America for the NGA-East project ([Frankel, 2015](#)). We compare spectral amplitudes from 46,178 ground-motion recordings at 1069 stations from 2873 earthquakes in the CEUS to the GMPEs. The ground-motion catalog is divided into potentially-induced and tectonic earthquakes using the classification scheme of [Petersen et al. \(2015\)](#), and their differences in geometric spreading are observed. We observe that the [Atkinson \(2015\)](#) GMPE is a good fit for ground motions at hypocentral distances of less than 60 km, and that the [Shahjoui and Pezeshk \(2016\)](#) GMPE captures the geometric spreading of ground motions at larger distances, for both induced and tectonic earthquakes.

*Electronic Supplement:* Figures for residuals, peak ground acceleration, spectral accelerations at the periods of 0.1 and 0.5 s, and peak ground velocity.

## INTRODUCTION

The level of seismicity in some parts of the central and eastern United States (CEUS) has increased markedly since ~2009 ([Ellsworth, 2013](#)), and this increase is cause for concern in terms of the seismic risk. Numerous studies linked this increased seismicity to disposal of oilfield wastewater by injection (e.g., [Horton, 2012](#); [Ellsworth, 2013](#); [Keranen et al., 2014](#);

[Hornbach et al., 2015](#); [Walsh and Zoback, 2015](#)), and hence it is referred to as induced or triggered seismicity.

An essential component of seismic hazard and risk assessment is the estimation of ground-motion amplitude from earthquakes, typically characterized by ground-motion prediction equations (GMPEs; [Kramer, 1996](#); [Bozorgnia and Bertero, 2004](#)). [Atkinson \(2015, hereafter, A15\)](#) developed a GMPE for small-to-moderate events at short hypocentral distances, with applications to induced seismicity. The GMPE was developed using ground motions from the Next Generation Attenuation-West2 (NGA-West2) project database ([Ancheta et al., 2013](#)) having event magnitudes from 3 to 6. Here, we evaluate the applicability of A15 and its assumption that the ground-motion amplitudes for small-to-moderate earthquakes are similar in the western United States and CEUS-induced earthquakes at short distances, using the ground motions collected from the CEUS. [Shahjoui and Pezeshk \(2016, hereafter, SP16\)](#) developed a GMPE for the CEUS, but it is applicable for magnitude 5–8 earthquakes, whereas most recent CEUS-induced earthquakes have been less than magnitude 5. For this reason, we evaluate the distance attenuation of SP16 and do not focus on magnitude scaling from the model for small magnitude earthquakes. SP16 uses an attenuation model that was developed for events in the CEUS (e.g., [Atkinson and Boore, 2014](#)); the SP16 attenuation of amplitudes with distance should thus be applicable over a broader distance range compared with the western United States model that is implicit in A15. [Yenier and Atkinson \(2015\)](#) also developed a regionally adjustable generic GMPE using a similar CEUS attenuation model and applied it to the ground motion in the central and eastern North America.

We classify the earthquakes into tectonic and induced earthquakes based on the regional classification of [Petersen et al. \(2015\)](#). We compare the amplitudes and their distance attenuation with the GMPEs separately for tectonic and in-

duced earthquakes. However, the induced and tectonic data sets are geographically separate for the most part, and hence we are not comparing events in otherwise identical conditions.

In the [Data Processing](#) section, we describe the collection and processing of CEUS ground-motion data. In the [Comparison of Ground Motions with the GMPEs](#) section, we compare the data with predictions from A15 and SP16. The comparison is carried out for the ground-motion intensity measures of peak ground velocity (PGV), peak ground acceleration (PGA), and 5% damped spectral accelerations (SAs) at periods of 0.2, 0.5, and 1.0 s ( $SA_{0.2}$ ,  $SA_{0.5}$ , and  $SA_{1.0}$ , respectively). Figures for  $SA_{0.2}$  are shown in this article, whereas other comparisons are provided in the [Ⓔ](#) electronic supplement to this article.

## DATA PROCESSING

### Ground-Motion Collection and Filtering

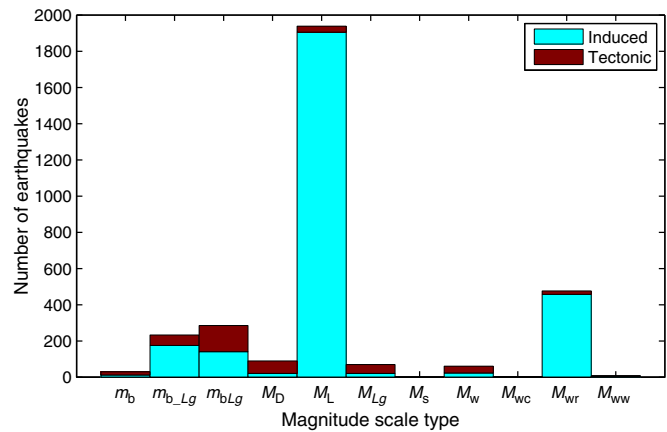
We compile a database of horizontal ground-motion acceleration time histories for all events with magnitudes  $\geq 3$  and epicentral distance  $\leq 200$  km from 1 January 2001 to 31 December 2016 for the CEUS region between  $27^\circ$  and  $55^\circ$  latitudes and  $-105^\circ$  and  $-70^\circ$  longitudes. The time histories are collected using the Standing Order for Data (SOD) tool developed by [Owens et al. \(2004\)](#). We did not collect data from nontelemeasured stations. Most of the recordings are obtained from GS, NX, N4, TA, YW, and OK station networks (with each of the networks providing  $> 1000$  recordings). Earthquake magnitudes, locations, and depths are collected from the U.S. Geological Survey (USGS) Advanced National Seismic System (ANSS) Comprehensive Earthquake Catalog (ComCat). More information about data sources is provided in [Data and Resources](#).

All time histories are baseline corrected by removing the mean and linear trend ([Boore and Bommer, 2005](#)). They are deconvolved using the *transferResponse* function provided in SOD. Time histories with signal-to-noise ratios (SNRs) of less than 2 are removed from further consideration. The noise is determined by considering the portion of the time history prior to *P*-wave arrival, as recorded by SOD. The SNR is computed by taking the ratio of the power of the signal-plus-noise portion with the noise portion ([Schultz, 2007](#)) and subtracting 1 ([Boore and Bommer, 2005](#)):

$$\text{SNR} = \frac{\int P_{\text{SN}}(\omega) d\omega}{\int P_{\text{N}}(\omega) d\omega} - 1, \quad (1)$$

in which  $P_{\text{SN}}(\omega)$  is the power spectral density of the signal-plus-noise portion and  $P_{\text{N}}(\omega)$  is that for the noise portion.

The remaining ground motions are filtered with an acausal fourth-order Butterworth filter with high-pass and low-pass frequencies of 0.3 and 20 Hz, respectively ([Boore and Bommer, 2005](#)). The response spectral values for most periods of interest (between 0.1 and 2 s) do not generally differ between the filtered and unfiltered ground motions, but the PGA and PGV values can be affected by filtering. The final ground-



▲ **Figure 1.** Number of earthquakes in various magnitude scales as per U.S. Geological Survey (USGS) Comprehensive Earthquake Catalog (ComCat) for events within the criteria of this article. The color version of this figure is available only in the electronic edition.

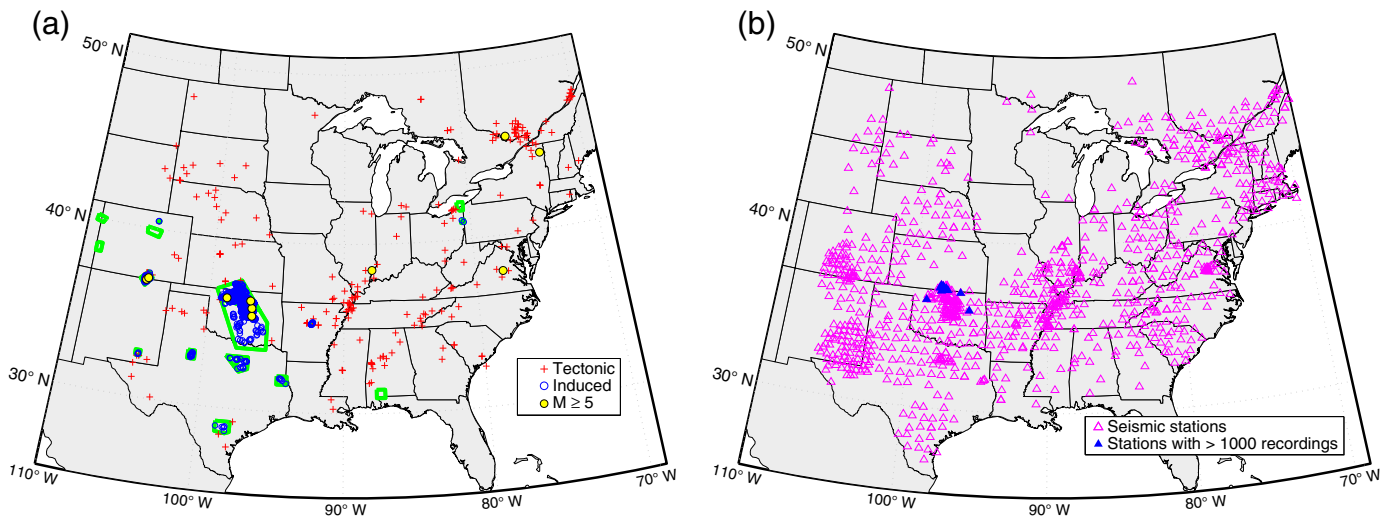
motion time series were spot checked, and all ground motions appeared visually reasonable.

For each multicomponent time history, we compute the median ground-motion spectral amplitudes across all non-redundant azimuths, referred to as RotD50 ([Boore, 2010](#)). All the later calculations and comparisons are done with this RotD50 metric of the acceleration time histories. After cleaning and filtering, we have a database of 46,178 ground-motion recordings at 1069 stations from 2873 earthquakes.

### Ground-Motion Magnitudes, Distances, and Classification as Induced or Tectonic

Earthquake magnitudes, locations, and depths are obtained from USGS ComCat (see [Data and Resources](#)). Earthquake coordinates and depths and recording station coordinates are then used to compute hypocentral distances for each ground motion. The magnitudes for different earthquakes are not provided in the same magnitude scale, depending on the catalog that supplied the event information. Figure 1 shows the count of earthquakes in different magnitude scales. Most magnitudes are computed in local magnitude ( $M_L$ ) or moment magnitude ( $M_w$ ,  $M_{wc}$ ,  $M_{wr}$ ,  $M_{ww}$ ) scales. There are also uncertainties in earthquake magnitudes and locations, due to the sparsity of seismic stations in the CEUS.

We distinguish ground motions originating from potentially-induced versus tectonic earthquakes for separate comparison with the GMPEs and to test for differences between the two. Potentially-induced earthquakes are classified using the regions of induced seismicity developed by the USGS ([Petersen et al., 2015, 2016](#)), as shown in Figure 2a. All other earthquakes are classified as tectonic. Although the attenuation of ground motions is different in the Gulf Coast region ([Hassani and Atkinson, 2015](#)), we do not separate them in this study. Because the focus of this study is on induced earthquakes, we do not expect a difference in conclusions by including Gulf Coast region motions. This classification results in 43,214 ground-motion recordings from 2609 induced earthquakes and 2964 recordings

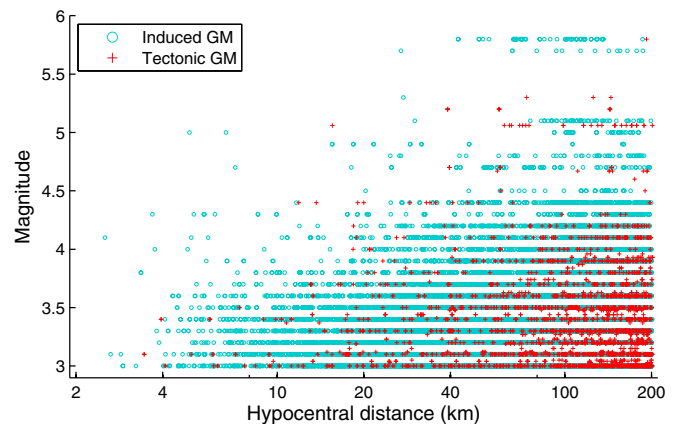


▲ **Figure 2.** (a) Locations of considered earthquakes. Polygons mark regions of induced seismicity identified by Petersen *et al.* (2015), and earthquakes within the polygons are classified as induced. (b) Locations of seismic stations that provided the recordings for the database. The color version of this figure is available only in the electronic edition.

from 264 tectonic earthquakes. There are six induced earthquakes and four tectonic earthquakes larger than magnitude 5, and these events are shown in Table 1. The earthquake magnitudes and distances to recordings are shown in Figure 3.

### Site-Effects Correction

Near-surface site effects are characterized here by the time-averaged shear-wave velocity in the upper 30 m of the site ( $V_{S30}$ ). For this study, we convert the observed ground-motion amplitudes to a site condition of  $V_{S30,ref} = 760$  m/s (the site condition considered by A15), using the site amplification model of Seyhan and Stewart (2014). Because we do not compare ground-motion amplitudes directly with SP16, we do not consider correction to the reference SP16 site condition of  $V_{S30} = 3000$  m/s. The ground motions do not have measured  $V_{S30}$  values at their associated recording sites, and hence we use estimated  $V_{S30}$  values calculated using topographic slope as a proxy for seismic site conditions (Wald and Allen, 2007). This



▲ **Figure 3.** Magnitudes and distances of the considered ground motions. The color version of this figure is available only in the electronic edition.

**Table 1**  
Earthquakes with  $M \geq 5$  in the Database

Date (yyyy/mm/dd)	Magnitude	Magnitude Type	Latitude (°)	Longitude (°)	Depth (m)	State	Classification
2002/04/20	5.3	$M_{Lg}$	44.512	-73.697	4,830	New York	Tectonic
2005/08/10	5.0	$M_{wc}$	36.947	-104.833	5,000	New Mexico	Induced
2008/04/18	5.2	$M_w$	38.452	-87.886	14,250	Illinois	Tectonic
2011/08/23	5.3	$M_{wr}$	37.063	-104.701	4,000	Colorado	Induced
2011/08/23	5.8	$M_w$	37.910	-77.936	20	Virginia	Tectonic
2011/11/06	5.7	$M_{vww}$	35.532	-96.765	5,200	Oklahoma	Induced
2013/05/17	5.06	$M_{Lg}$	45.757	-76.353	13,000	Quebec, Canada	Tectonic
2016/02/13	5.1	$M_{vww}$	36.490	-98.709	8,310	Oklahoma	Induced
2016/09/03	5.8	$M_{vww}$	36.425	-96.929	5,557	Oklahoma	Induced
2016/11/07	5.0	$M_{vww}$	35.991	-96.803	4,430	Oklahoma	Induced

$V_{S30}$  is approximate in that the estimated  $V_{S30}$  values are not precise, and the site amplification model used here was developed from NGA-West2 data and simulations, and hence it may not be applicable to the CEUS sites (Hassani and Atkinson, 2016). In the evaluations below, we consider these limitations by focusing on attenuation of ground motions and by examining a subset of data likely to have similar  $V_{S30}$  values.

## COMPARISON OF GROUND MOTIONS WITH THE GMPEs

We use the A15 and SP16 GMPEs for our comparisons. The A15 equation has been developed for ground motions from  $M_w$  3 to  $M_w$  6 earthquakes at hypocentral distances less than 40 km and for a reference site condition with  $V_{S30} = 760$  m/s. In the original paper, the equation has been extrapolated to distances up to 300 km, based on the decay provided by the NGA-West2 GMPE of Boore *et al.* (2013). The A15 equation is listed as follows:

$$\log Y = c_0 + c_1 M_w + c_2 M_w^2 + c \log R + c_4 R \quad (2)$$

and

$$R = \sqrt{R_{\text{hyp}}^2 + b_{\text{eff}}^2} \quad (3)$$

in which  $Y$  represents the median value of ground-motion intensity measure,  $M_w$  is the moment magnitude,  $R_{\text{hyp}}$  is the hypocentral distance,  $b_{\text{eff}}$  is the distance-saturation parameter, and  $c_i$  are coefficients described in Atkinson (2015).

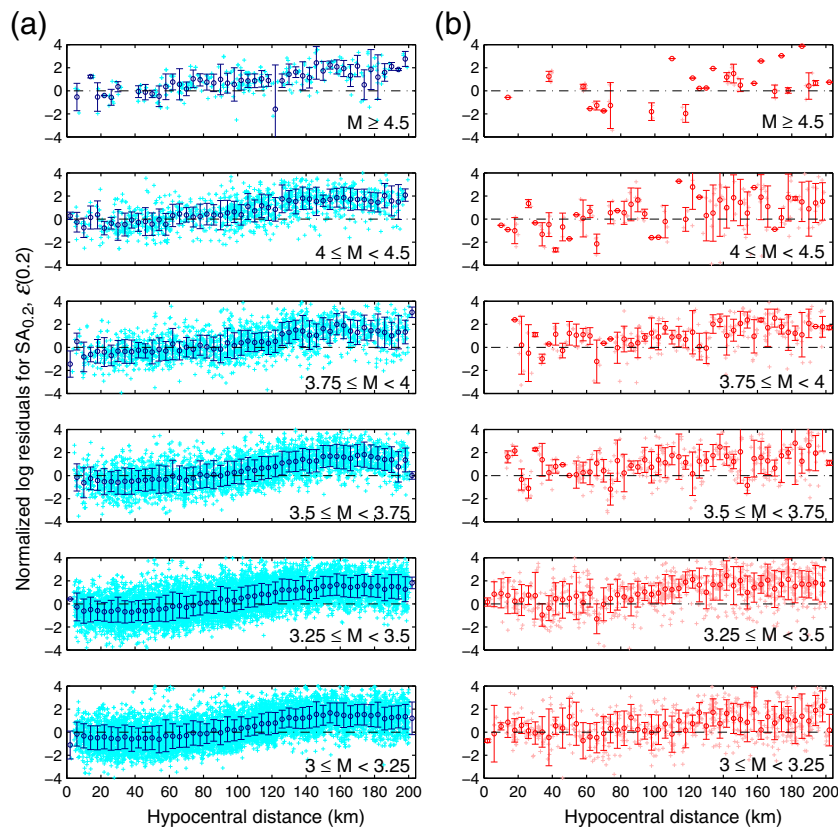
The SP16 GMPE has been developed for ground motions from  $M_w$  5– $M_w$  8 earthquakes in the 2–1000 km distance range and for the reference rock site condition with  $V_{S30} = 3000$  m/s (Hashash *et al.*, 2014). The SP16 equation is listed as follows:

$$\begin{aligned} \log \bar{Y} &= c_1 + c_2 M_w + c_3 M_w^2 + (c_4 + c_5 M_w) \\ &\times \min\{\log R, \log 60\} + (c_6 + c_7 M_w) \\ &\times \max\left\{\min\left\{\log \frac{R}{60}, \log \frac{120}{60}\right\}\right\} + (c_8 + c_9 M_w) \\ &\times \max\left\{\log \frac{R}{120}, 0\right\} + c_{10} R \end{aligned} \quad (4)$$

and

$$R = \sqrt{R_{\text{JB}}^2 + c_{11}^2} \quad (5)$$

in which  $\bar{Y}$  represents the median value of ground-motion intensity measure,  $M_w$  is the moment magnitude,  $R_{\text{JB}}$  is the Joyner–Boore distance (Joyner and Boore, 1981), and  $c_i$  are coefficients described in Shahjoui and Pezeshk (2016).



▲ **Figure 4.** Normalized log residuals for  $SA_{0.2}$  versus hypocentral distance for (a) induced and (b) tectonic earthquakes. Each row of the subplots contains residuals from earthquakes with the stated magnitude range. The mean and standard deviation of error bars are calculated using distance bins of  $\pm 4$  km centered at the marker. The color version of this figure is available only in the electronic edition.

## Computing Residuals

To aid comparisons across different earthquake magnitudes and source-to-site distances, we compute the normalized log residuals of the ground-motion intensity measures with respect to A15 predictions. Comparing residuals instead of the SAs allows us to eliminate the magnitude and distance dependence of the observations. This makes it visually easier to observe how the observations stack up against the GMPE. This allows us to plot multiple magnitude and multiple distance ranges on the same plot. Residual analysis also makes it easier to see the standard deviations of the data, which will be visually complex with a direct SA analysis.

The normalized log residual  $\varepsilon(\tau)$  is defined as the difference between the base-10 logarithms of the observed ground-motion amplitude and the predicted median ground-motion amplitude at period  $\tau$ , divided by the predicted log-standard deviation. Because the residuals have been normalized with respect to the standard deviation described in A15, the residuals are expected to follow a standard normal distribution (mean = 0 and standard deviation = 1) when the ground-motion ampli-

tudes follow the A15 GMPE. Based on the range of standard deviations provided for the A15 GMPE at different periods, a standard deviation of  $+\sigma$  or  $-\sigma$  for the normalized residuals implies an increase or decrease by a factor of 2–2.6 times in the ground-motion amplitude, respectively.

$$\varepsilon(\tau) = \frac{\log_{10} im_{\text{obs}}(\tau) - \log_{10} \overline{im}_{\text{A15}}(\tau)}{\sigma_{\text{total}, im_{\text{A15}}}(\tau)}, \quad (6)$$

in which  $im_{\text{obs}}(\tau)$  is the observed ground-motion amplitude at period  $\tau$ ,  $\overline{im}_{\text{A15}}$  is the median estimated amplitude, and  $\sigma_{\text{total}, im_{\text{A15}}}$  is the base-10 log-standard deviation in A15. Mixed-effects regression was also used to compute within- and between-event residuals, but the total residuals of equation (6) are considered in subsequent sections for simplicity and because the database is not particularly dominated by observations from individual earthquakes.

Residuals are not computed with respect to SP16 because of the inapplicability of this GMPE to the small-magnitude events used in this study.

### Variation of Residuals with Distance

Figure 4 shows the normalized residuals from equation (6) plotted versus distance and binned by magnitude and by induced or tectonic classification. Results are shown for 5% damped SAs at  $T = 0.2$  s, and similar results for other intensity measures are provided in the [E](#) electronic supplement. We observe that SAs for induced earthquakes are slightly below the A15 median predictions for hypocentral distances of  $R_{\text{hyp}} < 60$  km. This deviation appears to reduce at  $M \geq 4$ ; however, there are limited data in this large magnitude range. The observed SAs are higher than the predicted medians at larger distances. In general, the observed data are in agreement with A15 at short distances for which the GMPE is developed. However, the given extrapolation of A15 to larger distances does not accurately capture the attenuation-with-distance for these observations.

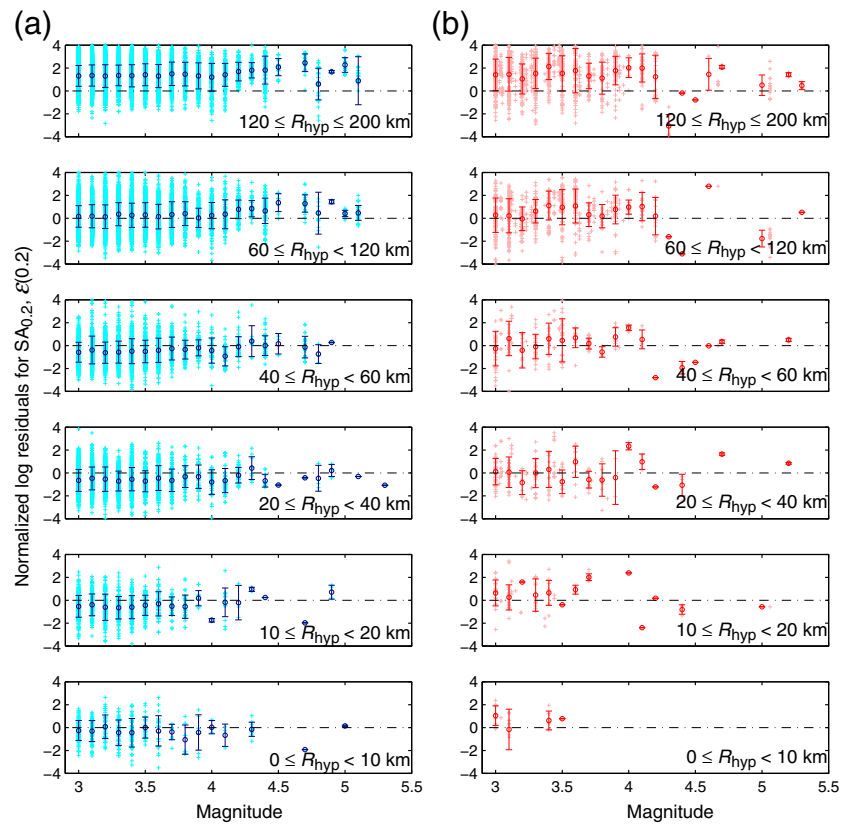
The observed ground motions are more limited for tectonic earthquakes, resulting in less clear trends with distance. From the limited data, it appears that the median SAs from tectonic earthquakes are larger than those from induced earthquakes for  $R_{\text{hyp}} \leq 60$  km. The pattern of residuals appears to be similar to that for induced earthquakes at larger distances. This indicates that, at a spectral period of  $T = 0.2$  s, the ground motions from tectonic earthquakes tend to be stronger than from induced earthquakes at shorter distances and tend to be similar at larger distances. We note that the induced or tectonic data sets are geographically separate for the most part, and hence we are not comparing events in otherwise identical conditions.

### Variation of Residuals with Magnitude

Figure 5 shows residuals from equation (6) plotted versus magnitude and binned by distance and by induced or tectonic classification. For a given bin, there is little or no trend with magnitude, indicating that A15 accurately captures the magnitude scaling of these ground-motion amplitudes. This figure again illustrates that the residuals are slightly below zero for  $R_{\text{hyp}} < 60$  km and above zero at larger distances. We also observe here that there is a reduction in induced-earthquake residual means going from the  $0 \leq R_{\text{hyp}} < 10$  km bin to the  $10 \leq R_{\text{hyp}} < 20$  km bin. This reduction is not observed for the tectonic earthquakes. This observation is consistent with the conclusions of Hough (2014) and Cremen *et al.* (2017) that ground-motion amplitudes for induced earthquakes reduce faster near source compared with those from tectonic earthquakes.

### Analysis of Attenuation with Distance

In this section, we compare A15 and SP16 with observed SAs to determine how well the GMPEs capture the geometric spreading with distance. To evaluate the SP16 model's attenuation prediction for lower magnitudes than the model is calibrated for, we scale the median SP16 prediction such that it



▲ **Figure 5.** Normalized log residuals for  $SA_{0.2}$  versus magnitude for (a) induced and (b) tectonic earthquakes. Each row of the subplots contains residuals from earthquakes with the stated hypocentral distance ( $R_{\text{hyp}}$ ) range. The mean and standard deviation of error bars are calculated at each indicated magnitude. The color version of this figure is available only in the electronic edition.

Table 2 Coefficients for the Scale Factor to Obtain SP16 <sub>scaled</sub> from the SP16 GMPE			
<i>T</i> (s)	<i>s</i> <sub>0</sub>	<i>s</i> <sub>1</sub>	<i>s</i> <sub>2</sub>
PGV	-0.1719	0.1423	-0.0212
PGA	-3.2598	0.9594	-0.0756
0.010	-3.3551	1.0352	-0.0825
0.020	-4.4872	1.3210	-0.1036
0.030	-4.8481	1.4103	-0.1104
0.040	-4.8257	1.4209	-0.1122
0.050	-4.7079	1.4042	-0.1118
0.075	-4.3518	1.3340	-0.1066
0.100	-3.9355	1.2456	-0.1004
0.150	-3.3118	1.0459	-0.0815
0.200	-2.7497	0.8790	-0.0665
0.250	-2.4641	0.7911	-0.0592
0.300	-2.2040	0.7148	-0.0531
0.400	-1.9925	0.6608	-0.0496
0.500	-1.8128	0.6192	-0.0472
0.750	-0.7713	0.2049	-0.0056
1.000	-0.0604	-0.0732	0.0223
1.500	0.8008	-0.3951	0.0521
2.000	1.3401	-0.5957	0.0707
3.000	2.6979	-1.1047	0.1195
4.000	2.8988	-1.1207	0.1182
5.000	3.0108	-1.1163	0.1157

SP16, [Shahjoui and Pezeshk \(2016\)](#); GMPE, ground-motion prediction equation; PGA, peak ground acceleration; PGV, peak ground velocity.

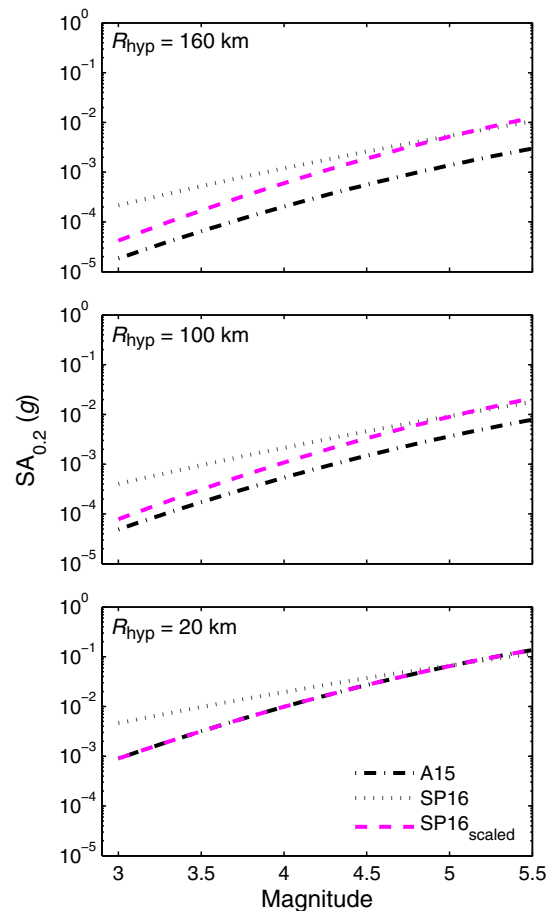
equals that from A15 at a hypocentral distance of 20 km, as shown in equation (7), and denote the result SP16<sub>scaled</sub>

$$\begin{aligned} \overline{im}_{SP16scaled}(M, R_{hyp}) &= \frac{\overline{im}_{A15}(M, R_{hyp} = 20 \text{ km})}{\overline{im}_{SP16}(M, R_{hyp} = 20 \text{ km})} \\ &\times \overline{im}_{SP16}(M, R_{hyp}), \end{aligned} \quad (7)$$

in which  $\overline{im}_{A15}(M, R_{hyp})$  is the median predicted intensity measure for A15 at magnitude  $M$ , and hypocentral distance  $R_{hyp}$ ,  $\overline{im}_{SP16}(M, R_{hyp})$ , and  $\overline{im}_{SP16scaled}(M, R_{hyp})$  are the corresponding predictions for SP16 and SP16<sub>scaled</sub>, respectively.

The scaled GMPE SP16<sub>scaled</sub> can be calculated using the following:

$$\begin{aligned} \log \bar{Y} &= s + \log \bar{Y}_{SP16} \\ \log \bar{Y} &= s + c_1 + c_2M + c_3M^2 \\ &+ (c_4 + c_5M) \times \min\{\log R, \log 60\} \\ &+ (c_6 + c_7M) \times \max\left\{\min\left\{\log \frac{R}{60}, \log \frac{120}{60}\right\}\right\} \\ &+ (c_8 + c_9M) \times \max\left\{\log \frac{R}{120}, 0\right\} + c_{10}R \end{aligned} \quad (8)$$



▲ **Figure 6.** Median SA<sub>0.2</sub> values predicted by the ground-motion prediction equations (GMPEs) for three hypocentral distances, as indicated on each subplot. The color version of this figure is available only in the electronic edition.

and

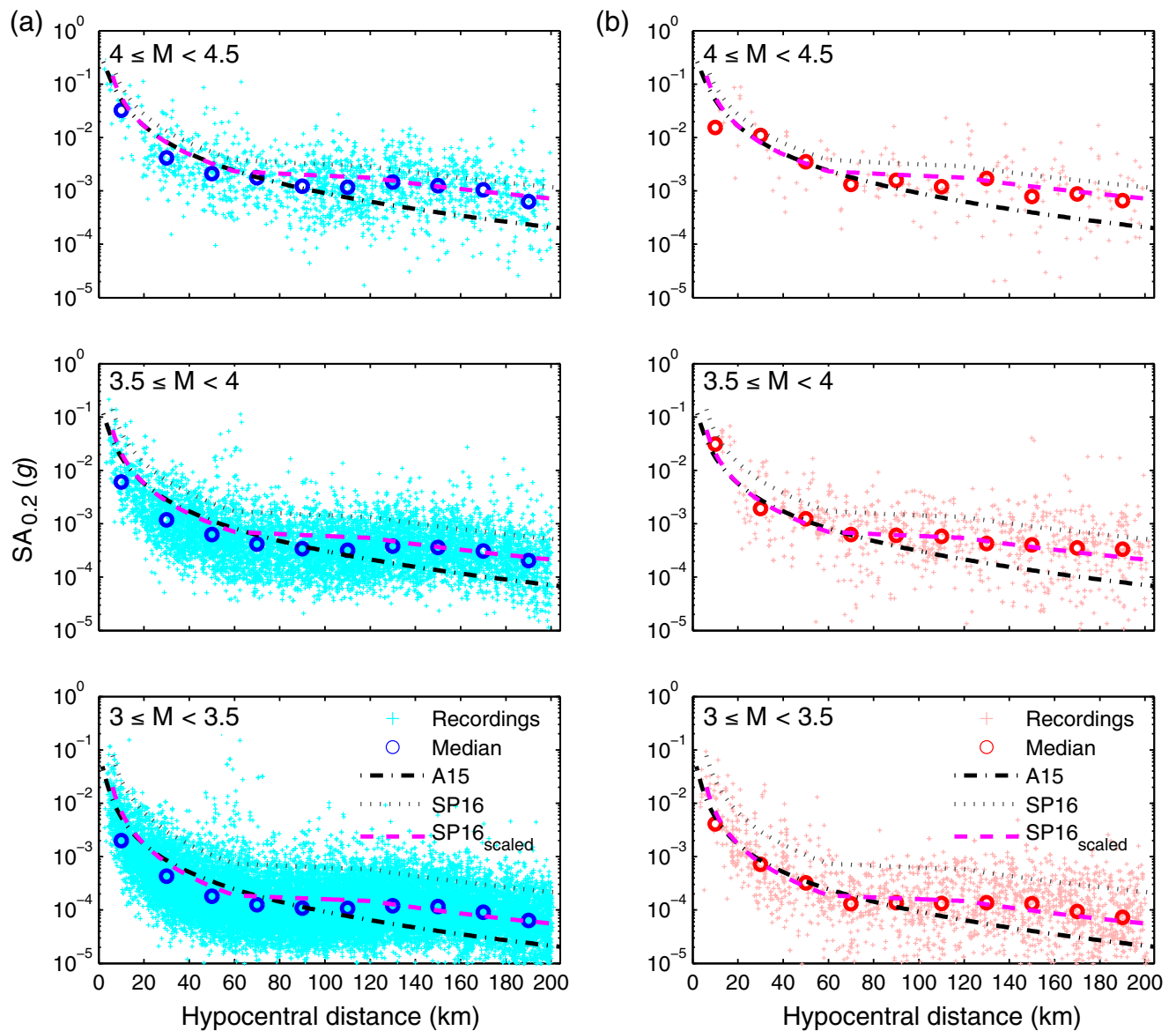
$$R = \sqrt{R_{JB}^2 + c_{11}^2}, \quad (9)$$

in which the coefficients  $c_1$  to  $c_{11}$  are described in [Shahjoui and Pezeshk \(2016\)](#), and  $s$  is calculated using equation (10). The log values are base-10.

$$s = s_0 + s_1M + s_2M^2. \quad (10)$$

The coefficients  $s_0$ ,  $s_1$ , and  $s_2$  are given in Table 2. The scaled equation (8) represents a composite model that maintains the overall amplitude levels at 20 km and magnitude scaling of A15 and follows the SP16 attenuation function.

Equation (8) uses the closest horizontal distance to the vertical projection of the rupture plane ( $R_{JB}$ ) instead of hypocentral distance. To convert  $R_{hyp}$  to  $R_{JB}$ , we assume that all earthquakes have a point source rupture at a depth of 5 km. Then,  $R_{JB} = \sqrt{R_{hyp}^2 - 5^2}$ . This assumption has some impact on predictions for  $R_{hyp} < 20$  km but little impact at larger distances.



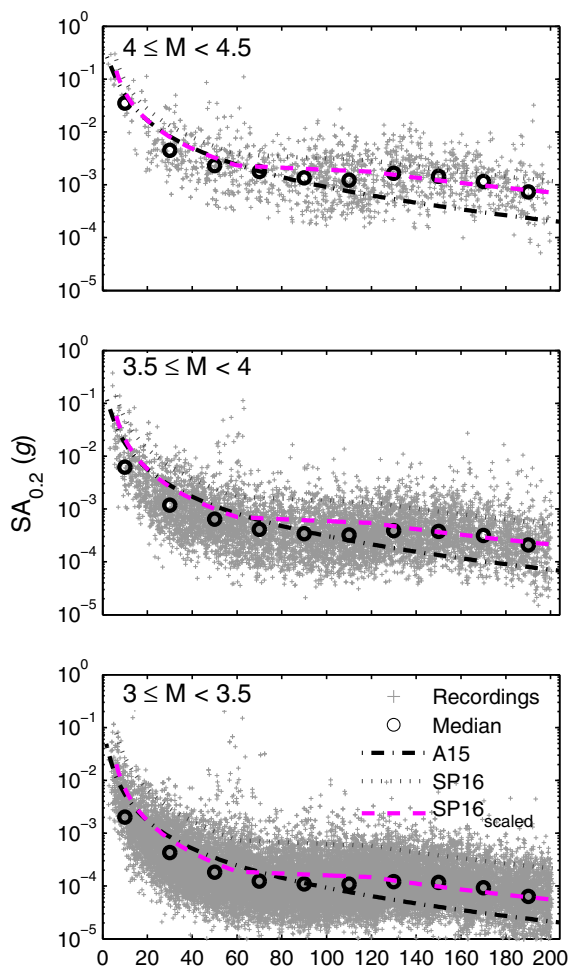
▲ **Figure 7.** Observed  $SA_{0.2}$  values for (a) induced and (b) tectonic earthquakes, with median estimated accelerations from A15 and SP16. Each row of the subplots includes observations from the stated magnitude range. GMPEs are evaluated at the middle of the magnitude bins. The color version of this figure is available only in the electronic edition.

Figure 6 illustrates the impact of this scaling approach by showing the A15, SP16, and SP16<sub>scaled</sub> predictions for various magnitudes and distances. At  $R_{hyp} = 20$  km, SP16<sub>scaled</sub> is equivalent to A15 because of scaling at this distance. At larger distances, SP16<sub>scaled</sub> predicts smaller amplitudes than SP16 (because of the A15 magnitude scaling) but larger amplitudes than A15 (because of the SP16 attenuation model). At larger magnitudes, SP16<sub>scaled</sub> and SP16 are equivalent.

Figure 7 shows the variation of observations and GMPEs with distance for three magnitude ranges. SP16 is stated to be applicable for  $R_{JB} > 2$  km, so SP16 and SP16<sub>scaled</sub> are plotted only for  $R_{hyp} > \sqrt{5^2 + 2^2} = 5.4$  km. The predicted ground motions for A15 and SP16<sub>scaled</sub> are similar at  $R_{hyp} < 60$  km. Differences for  $R_{hyp} > 60$  km result from

SP16's lower rate of attenuation from 60 to 120 km. We observe that the SP16<sub>scaled</sub> better predicts the attenuation of the observed ground motions for both induced and tectonic ground motions. A15 captures the ground-motion behavior well at  $R_{hyp} < 60$  km because it was developed for short distances; however, the distance attenuation of Boore *et al.* (2013) from NGA-West2 used in this GMPE for larger distances does not capture well the observed attenuation.

Figure 8 shows the variation of SAs only for ground motions recorded in Texas, Oklahoma, and Kansas (i.e., latitudes between 30° and 40°, and longitudes between -103° and -94°). Most of the induced earthquakes have occurred in this region (Weingarten *et al.*, 2015), and this region is expected to have similar site characteristics, thus reducing the impacts from



▲ **Figure 8.** Observed  $SA_{0.2}$  values from Texas, Oklahoma, and Kansas, with median estimated accelerations from A15 and SP16. Each subplot includes observations from the stated magnitude range and GMPE predictions for the middle of the magnitude bin. The color version of this figure is available only in the electronic edition.

spatial variation of  $V_{S30}$  estimates in observations or predictions. We observe similar behavior as for the full data set (i.e., SP16 captures geometric spreading well, whereas A15 captures the amplitudes well for  $R_{hyp} \leq 60$  km).

### Observations for Other Intensity Measures

Results similar to those from Figures 4 through 8, for ground-motion spectral amplitudes at other periods, are provided in the  electronic supplement and briefly summarized here. Additionally, Figures 9 and 10 summarize the variation of residuals with respect to distance and magnitude, respectively, at all periods of consideration.

For all intensity measures, the residuals with respect to A15 increase between  $\sim 60$  and 130 km and then remain constant at larger distances. There is no significant magnitude variation in the residuals for both induced and tectonic earthquakes. These observations are very similar to those in Figures 4 through 8. For induced ground motions at PGA, A15 has

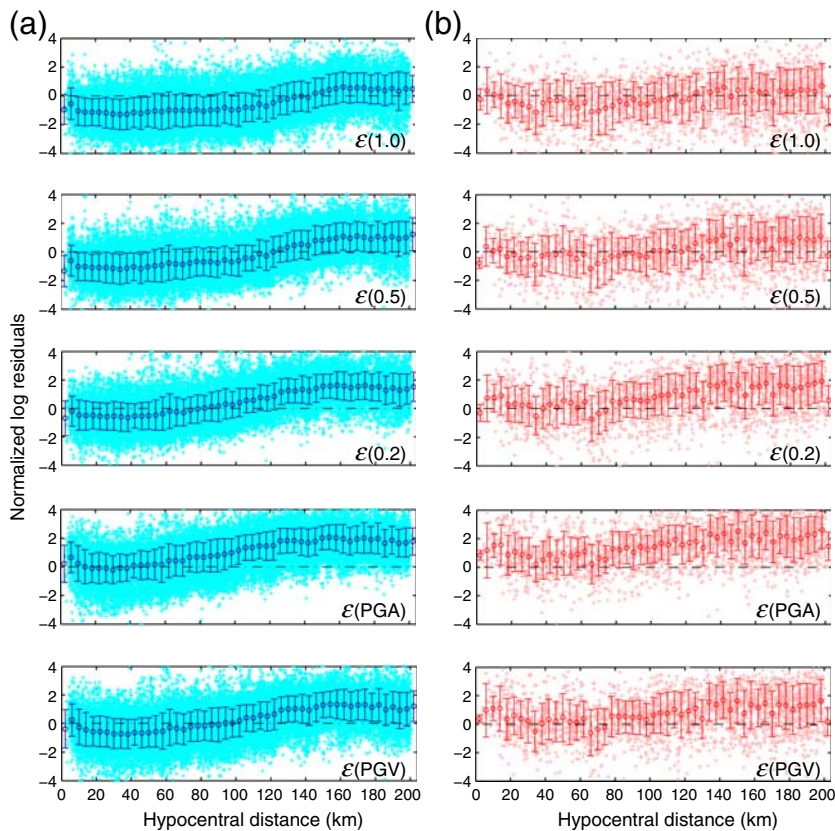
a tendency to slightly underpredict observed SAs for  $R_{hyp} \leq 60$  km. In the same distance range,  $SA_{0.5}$  and  $SA_{1.0}$  predictions are higher than observed SAs. However, these deviations reduce at larger magnitudes, which would be the earthquakes of interest for structures at these higher periods. The behavior for PGV is similar to that for  $SA_{0.2}$ . In no cases are the underpredictions or overpredictions as substantial as the attenuation-related deviations, and these underpredictions and overpredictions may be a result of the period-dependent site-effects modifications rather than A15, so these observations do not clearly indicate any shortcoming of the A15 model.

For all intensity measures, it appears that the amplitudes from tectonic earthquakes are slightly higher than those from induced earthquakes at  $R_{hyp} \leq 60$  km and similar to those from induced earthquakes at larger distances. However, most of the induced earthquakes occurred in the central United States, whereas the tectonic earthquakes occurred primarily in the eastern United States, so the differences between induced or tectonic data sets could be due to regional difference in geology as well as the origin. Additionally, the differences may also be due to the dependence of earthquake source parameters on focal depth, as shown by Yenier and Atkinson (2015) and Atkinson and Assatourians (2017).

The attenuation of ground-motion amplitudes with distance is better modeled by SP16 and  $SP16_{scaled}$  than by A15 for all periods. This aligns with our earlier observation that observed data are in agreement with A15 at short distances for which the GMPE is developed. However, the given extrapolation of A15 to larger distances does not accurately capture the attenuation-with-distance for these observations. For all metrics besides PGA, the  $SP16_{scaled}$  model captures both distance attenuation and magnitude scaling well. For PGA, the amplitudes appear to attenuate at an even slower rate with distance than SP16 and  $SP16_{scaled}$  predict. This pattern remains when focusing only on ground motions recorded in Texas, Oklahoma, and Kansas.

## CONCLUSIONS

We assessed the applicability of A15 GMPE on ground motions compiled for magnitude  $\geq 3$  earthquakes occurring from 2001 to 2016 in the CEUS. A comparison with the CEUS ground motions was undertaken because the GMPE was developed using the NGA-West2 database of earthquakes primarily from the western North America. We also compared the attenuation-with-distance predicted by the SP16 model with the observed ground motions. Evaluations were performed for the ground-motion metrics PGA, PGV,  $SA_{0.2}$ ,  $SA_{0.5}$ , and  $SA_{1.0}$ . The ground motions were classified as potentially induced or tectonic based on the region of occurrence of the associated earthquake using the classification scheme of Petersen *et al.* (2015). The induced and tectonic data sets are geographically separate for the most part, and hence we are not comparing events in otherwise identical conditions. Our analysis is also not well constrained for  $M > 4.5$ , due to very limited data at these larger magnitudes.



▲ **Figure 9.** Normalized log residuals for specified periods versus hypocentral distance for (a) induced and (b) tectonic earthquakes. Each row of the subplots contains spectral amplitude residuals at the stated period and for all earthquake magnitudes. The mean and standard deviation of error bars are calculated using distance bins of  $\pm 4$  km centered at the marker. The color version of this figure is available only in the electronic edition.

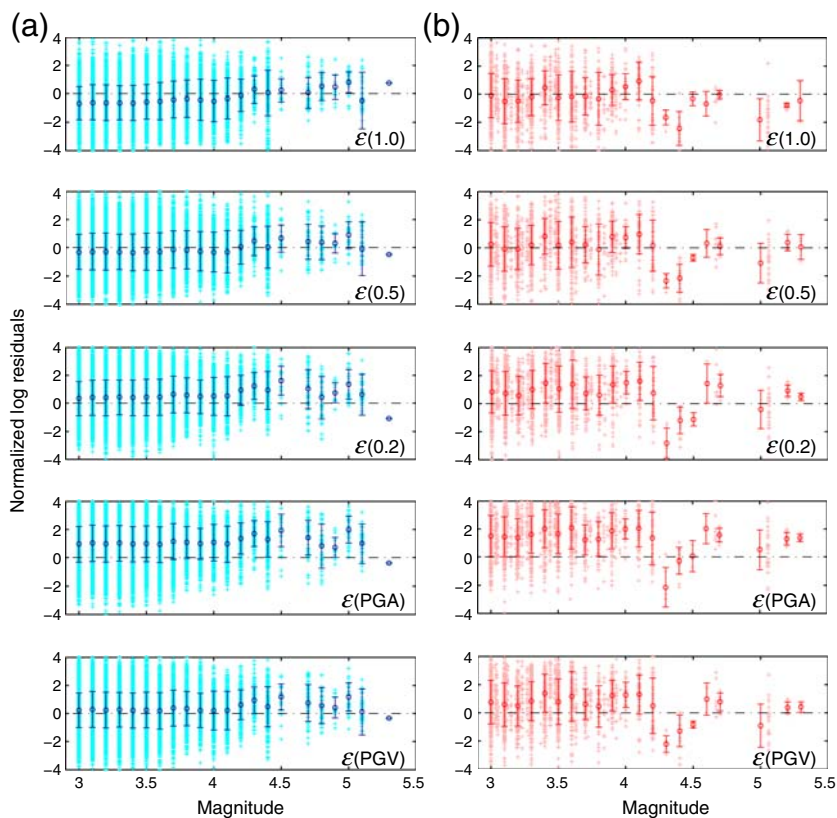
It was observed that comparison of ground-motion spectral amplitudes for induced earthquakes with A15 varies by period. For, PGA, PGV, and  $SA_{0.2}$ , A15 is consistent with observations for  $R_{hyp} < 60$  km and underestimates observations at larger distances. At longer periods ( $SA_{0.5}$  and  $SA_{1.0}$ ), A15 overestimates the SAs when  $R_{hyp} \leq 60$  km, but they are closer to observations at larger distances. This deviation appears to reduce at  $M \geq 4$ , and the amplitudes for these longer-period SAs are extremely small (usually  $< 10^{-3}$  g) for most of the ground motions considered and hence are of little engineering relevance. In general, A15 captures well the attenuation of ground motions for  $R_{hyp} \leq 60$  km but does not capture the lower rate of attenuation at larger distances. In contrast, SP16 has an additional term for the lower rate of attenuation between 60 and 120 km and is able to capture the attenuation better at all periods, except at PGA (where observations attenuate more slowly than predictions).

Comparing the recordings from induced earthquakes with those from tectonic earthquakes, we observe that the former amplitudes reduce faster within the first 20 km of the source. This is consistent with observations of Hough (2014) and Cre-

men *et al.* (2017), who used the ground-motion intensities from “Did You Feel It?” data for their comparisons. Additionally, the ground motions from tectonic earthquakes appear to have slightly higher amplitudes than those from induced earthquakes for  $R_{hyp} \leq 60$  km and similar amplitudes at larger distances.

In general, we observe that A15 captures well the magnitude scaling of the ground-motion amplitudes for small-magnitude earthquakes and their distance attenuation at short hypocentral distances. The A15 model was developed with the assumption that amplitudes from small-to-moderate-induced earthquakes in the CEUS are similar to those for tectonic earthquakes in the western North America at  $R_{hyp} \leq 40$  km. Our analysis indicates that this is a valid assumption. A15 also described an additional term in their GMPE that allows it to be applicable for  $40 \text{ km} < R_{hyp} \leq 300$  km, based on amplitude decay provided by the NGA-West2 GMPE of Boore *et al.* (2013). From the observations in this study, that additional term does not capture the lower rate of attenuation in the CEUS, which is captured better by SP16. We suggest that caution should be exercised when using A15 for  $R_{hyp} > 60$  km. We propose here the  $SP16_{scaled}$  GMPE obtained by combining the amplitudes predicted by A15 at short distances and the distance attenuation of SP16. This proposed GMPE better captures both the ground-motion amplitudes and attenuation to 200 km than either of the individual GMPEs.

It is possible that the difference in the behavior of observed ground motions for various intensity measures are a result of the period-dependent  $V_{S30}$  correction performed for this study. There are uncertainties associated with applying this correction to the CEUS, which can manifest in incorrect scaling of ground motions at different periods. It is also possible that this correction resulted in the differences that we observed in ground motions from induced and tectonic earthquakes. Most of the induced earthquakes occurred in the central United States, whereas the tectonic earthquakes occurred primarily in the eastern United States, so a regional difference in geology, rather than the earthquake rupture process, could explain some of the observed differences. Other factors that we did not fully account for in this study are the differences in magnitude scales and location uncertainties of the CEUS earthquakes. We also did not evaluate the influence of focal depth on the observed differences in amplitudes. Yenier and Atkinson (2015) and Atkinson and Assatourians (2017) note that earthquake stress drops increase with increasing depth and have attributed the difference in tectonic-versus-induced ground-motion amplitudes to this factor. Development of more detailed site information at seismic stations in the CEUS, and



▲ **Figure 10.** Normalized log residuals for specified periods versus magnitude for (a) induced and (b) tectonic earthquakes. Each row of the subplots contains spectral amplitude residuals at the stated period and at all hypocentral distances. The mean and standard deviation of error bars are calculated at each indicated magnitude. The color version of this figure is available only in the electronic edition.

development of a validated site amplification model, would help resolve some of the above uncertainties. Development of an induced seismicity GMPE for Texas, Oklahoma, and Kansas might also be useful in addressing region-specific effects and may be justified in this situation, given the substantial available ground-motion data. The location and depth uncertainties associated with the earthquake sources limit GMPE evaluations at very short distances and are more difficult to resolve without development of improved hypocentral location accuracy in the region.

## DATA AND RESOURCES

Ground-motion data were collected from Incorporated Research Institutions for Seismology (IRIS) Data Services (<http://ds.iris.edu/ds/nodes/dmc/>, last accessed May 2017) through the interface provided by the Standing Order of Data (SOD; Owens *et al.*, 2004). The facilities of IRIS Data Services (DS), and specifically the IRIS Data Management Center, were used for access to waveform, metadata, or products required in this study. The IRIS DS is funded through the National Science Foundation and specifically the GEO Directorate through the Instrumentation and Facilities Program of the Na-

tional Science Foundation under Cooperative Agreement EAR-1063471. Some activities are supported by the National Science Foundation EarthScope Program under Cooperative Agreements EAR-0733069 and EAR-1261681.

We considered earthquakes with magnitude  $\geq 3$ , between latitudes  $27^\circ$  to  $55^\circ$  and longitudes  $-105^\circ$  to  $-70^\circ$  and occurring between 1 January 2001 to 31 December 2016. The ground motions were collected from broadband velocity seismic stations and accelerometers with component codes HH, HL, HN and BH, BL, BN, with sample rates between 40 and 200 Hz and within 200 km of an earthquake. We did not collect data from nontelemetered stations. The earthquake magnitudes, locations, and depths were updated from those provided by SOD to those provided in the U.S. Geological Survey (USGS) Advanced National Seismic System (ANSS) Composite Catalog (<http://earthquake.usgs.gov/data/comcat/>, last accessed January 2017). These data were collected on 24 January 2017.

The database of ground motions used in this study is available at [https://github.com/abhineetgupta/groundMotionsDatabase\\_CEUS](https://github.com/abhineetgupta/groundMotionsDatabase_CEUS) (last accessed May 2017).

Supplementary plots for residuals corresponding to peak ground acceleration (PGA), peak ground velocity (PGV), and spectral accelerations (i.e.,  $SA_{0.5}$  and  $SA_{1.0}$ ) are provided in the  electronic supplement to this article.

## ACKNOWLEDGMENTS

Funding for this work came from the Stanford Center for Induced and Triggered Seismicity. We would like to thank Gregory Beroza for guidance on ground-motion data collection. The constructive comments of Gail Atkinson, an anonymous reviewer, and Eastern Section Editor Martin C. Chapman are gratefully acknowledged. 

## REFERENCES

- Ancheta, T. D., R. B. Darragh, J. P. Stewart, E. Seyhan, W. J. Silva, B. S. Chiou, K. E. Wooddell, R. W. Graves, A. R. Kottke, D. M. Boore, *et al.* (2013). PEER NGA-West2 Database, *PEER Report No. 2013/03*, University of California, Berkeley.
- Atkinson, G. M. (2015). Ground-motion prediction equation for small-to-moderate events at short hypocentral distances, with application to induced seismicity hazards, *Bull. Seismol. Soc. Am.* **105**, no. 2A, 981–992.
- Atkinson, G. M., and K. Assatourians (2017). Are ground-motion models derived from natural events applicable to the estimation of expected motions for induced earthquakes? *Seismol. Res. Lett.* **88**, no. 2A, 430–441.
- Atkinson, G. M., and D. M. Boore (2014). The attenuation of Fourier amplitudes for rock sites in eastern North America, *Bull. Seismol. Soc. Am.* **104**, no. 1, 513–528.

- Boore, D. M. (2010). Orientation-independent, nongeometric-mean measures of seismic intensity from two horizontal components of motion, *Bull. Seismol. Soc. Am.* **100**, no. 4, 1830–1835.
- Boore, D. M., and J. J. Bommer (2005). Processing of strong-motion accelerograms: Needs, options and consequences, *Soil Dynam. Earthq. Eng.* **25**, no. 2, 93–115.
- Boore, D. M., J. P. Stewart, E. Seyhan, and G. M. Atkinson (2013). PEER NGA-West2 equations for predicting PGA, PGV, and 5% damped PSA for shallow crustal earthquakes, *Earthq. Spectra* **30**, no. 3, 1057–1085.
- Bozorgnia, Y., and V. V. Bertero (2004). *Earthquake Engineering: From Engineering Seismology to Performance-Based Engineering*, CRC Press, Boca Raton, Florida.
- Bozorgnia, Y., N. A. Abrahamson, L. A. Atik, T. D. Ancheta, G. M. Atkinson, J. W. Baker, A. Baltay, D. M. Boore, K. W. Campbell, B. S.-J. Chiou, *et al.* (2014). NGA-West2 Research Project, *Earthq. Spectra* **30**, no. 3, 973–987.
- Cremon, G., A. Gupta, and J. W. Baker (2017). Evaluation of ground motion intensities from induced earthquakes using “Did You Feel It?” data, *16th World Conf. on Earthquake Engineering*, Santiago, Chile, 12 January.
- Ellsworth, W. L. (2013). Injection-induced earthquakes, *Science* **341**, no. 6142, 1225–1242.
- Frankel, A. D. (2015). PEER NGA-East: Median ground-motion models for the central and eastern North America region, *PEER Report No. 2015/04*, University of California, Berkeley.
- Hashash, Y. M. A., A. R. Kottke, J. P. Stewart, K. W. Campbell, B. Kim, C. Moss, S. Nikolaou, E. M. Rathje, and W. J. Silva (2014). Reference rock site condition for central and eastern North America, *Bull. Seismol. Soc. Am.* **104**, no. 2, 684–701.
- Hassani, B., and G. M. Atkinson (2015). Referenced empirical ground-motion model for eastern North America, *Seismol. Res. Lett.* **86**, no. 2A, 477–491.
- Hassani, B., and G. M. Atkinson (2016). Applicability of the NGA-West2 site-effects model for central and eastern North America, *Bull. Seismol. Soc. Am.* **106**, no. 3, 1331–1341.
- Hornbach, M. J., H. R. DeShon, W. L. Ellsworth, B. W. Stump, C. Hayward, C. Frohlich, H. R. Oldham, J. E. Olson, M. B. Magnani, C. Brokaw, *et al.* (2015). Causal factors for seismicity near Azle, Texas, *Nat. Comm.* **6**, 6728.
- Horton, S. (2012). Disposal of hydrofracking waste fluid by injection into subsurface aquifers triggers earthquake swarm in Central Arkansas with potential for damaging earthquake, *Seismol. Res. Lett.* **83**, no. 2, 250–260.
- Hough, S. E. (2014). Shaking from injection-induced earthquakes in the central and eastern United States, *Bull. Seismol. Soc. Am.* **104**, no. 5, 2619–2626.
- Joyner, W. B., and D. M. Boore (1981). Peak horizontal acceleration and velocity from strong-motion records including records from the 1979 imperial valley, California, earthquake, *Bull. Seismol. Soc. Am.* **71**, no. 6, 2011–2038.
- Keranen, K. M., M. Weingarten, G. A. Abers, B. A. Bekins, and S. Ge (2014). Sharp increase in central Oklahoma seismicity since 2008 induced by massive wastewater injection, *Science* **345**, no. 6195, 448–451.
- Kramer, S. L. (1996). *Geotechnical Earthquake Engineering*, Prentice Hall, Upper Saddle River, New Jersey.
- Owens, T. J., H. P. Crotwell, C. Groves, and P. Oliver-Paul (2004). SOD: Standing Order for Data, *Seismol. Res. Lett.* **75**, no. 4, 515–520.
- Petersen, M. D., C. S. Mueller, M. P. Moschetti, S. M. Hoover, A. L. Llenos, W. L. Ellsworth, A. J. Michael, J. L. Rubinstein, A. F. McGarr, and K. S. Rukstales (2016). 2016 one-year seismic hazard forecast for the central and eastern United States from induced and natural earthquakes, *U.S. Geol. Surv. Open-File Rept. 2016-1035*, available at <http://pubs.er.usgs.gov/publication/ofr20161035> (last accessed September 2016).
- Petersen, M. D., C. S. Mueller, M. P. Moschetti, S. M. Hoover, J. L. Rubinstein, A. L. Llenos, A. J. Michael, W. L. Ellsworth, A. F. McGarr, and A. A. Holland (2015). Incorporating induced seismicity in the 2014 United States National Seismic Hazard Model—Results of 2014 workshop and sensitivity studies, *U.S. Geol. Surv. Open-File Rept. 2015-1070*.
- Schultz, S. (2007). Signal-to-noise ratio in neuroscience, *Scholarpedia* **2**, no. 6, 2046.
- Seyhan, E., and J. P. Stewart (2014). Semi-empirical nonlinear site amplification from NGA-West2 data and simulations, *Earthq. Spectra* **30**, no. 3, 1241–1256.
- Shahjoui, A., and S. Pezeshk (2016). Alternative hybrid empirical ground-motion model for central and eastern North America using hybrid simulations and NGA-West2 models, *Bull. Seismol. Soc. Am.* **106**, no. 2, 734–754.
- Wald, D. J., and T. I. Allen (2007). Topographic slope as a proxy for seismic site conditions and amplification, *Bull. Seismol. Soc. Am.* **97**, no. 5, 1379–1395.
- Walsh, F. R., and M. D. Zoback (2015). Oklahoma’s recent earthquakes and saltwater disposal, *Sci. Adv.* **1**, no. 5, e1500195.
- Weingarten, M., S. Ge, J. W. Godt, B. A. Bekins, and J. L. Rubinstein (2015). High-rate injection is associated with the increase in U.S. mid-continent seismicity, *Science* **348**, no. 6241, 1336–1340.
- Yenier, E., and G. M. Atkinson (2015). Regionally adjustable generic ground-motion prediction equation based on equivalent point-source simulations: Application to central and eastern North America, *Bull. Seismol. Soc. Am.* **105**, no. 4, 1989–2009.

*Abhineet Gupta*

*Department of Civil and Environmental Engineering  
Stanford University  
Blume Center  
Building 540, 439 Panama Mall, Room 206  
Stanford, California 94305 U.S.A.  
abhineet.stanford@gmail.com*

*Jack W. Baker*

*Department of Civil and Environmental Engineering  
Stanford University  
473 Via Ortega, Room 283  
Stanford, California 94305-4020 U.S.A.*

*William L. Ellsworth*

*Department of Geophysics  
Stanford University  
Mitchell Building, 397 Panama Mall, Room 373B  
Stanford, California 94305 U.S.A.*

Published Online 28 June 2017